Environmental Science & Technology

Article

pubs.acs.org/est

Siderophore and Organic Acid Promoted Dissolution and Transformation of Cr(III)-Fe(III)-(oxy)hydroxides

Emily M. Saad,[†] Jingying Sun,[‡] Shuo Chen,[‡] Olaf J. Borkiewicz,[§] Mengqiang Zhu,[∥] Owen W. Duckworth,[⊥] and Yuanzhi Tang*[,†]

[†]School of Earth and Atmospheric Sciences, Georgia Institute of Technology, Atlanta, Georgia 30332-0340, United States

[‡]Department of Physics and Texas Center for Superconductivity (TCSUH), University of Houston, Houston, Texas 77204, United States

[§]Advanced Photon Source, Argonne National Laboratory, Argonne, Illinois 60439, United States

[∥]Department of Ecosystem Science and Management, University of Wyoming, Laramie, Wyoming 82071, United States

[⊥]Department of Crop and Soil Science, North Carolina State University, Raleigh, North Carolina 27695, United States

Supporting Information

ABSTRACT: The role of microbial activities on the transformation of chromium (Cr) remediation products has generally been overlooked. This study investigated the stability of Cr(III)-Fe(III)-(oxy)hydroxides, common Cr(VI) remediation products, with a range of compositions in the presence of common microbial exudates, siderophores and small organic acids. In the presence of a representative siderophore, desferrioxamine B (DFOB), iron (Fe) was released at higher rates and to greater extents relative to Cr from all solid phases. The presence of oxalate alone caused the release of Cr, but not of Fe, from all solid phases. In the presence of both DFOB and oxalate, oxalate acted synergistically with DFOB to increase the Fe, but not the Cr, release rate. Upon reaction with DFOB or DFOB + oxalate, the remaining solids became enriched in Cr relative to Fe. Such incongruent dissolution led to solid phases with different compositions and increased solubility relative to the initial solid phases. Thus, the presence of microbial exudates can promote the release of Cr(III) from remediation products via both ligand complexation and increased solid solubility. Understanding the potential reaction kinetics and pathways of Cr(VI) remediation products in the presence of microbial activities is necessary to assess their long-term stability.

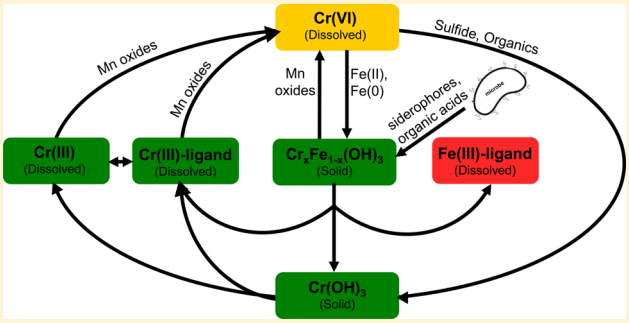

1. INTRODUCTION

Chromium (Cr) is a significant contaminant in the United States[1] and around the globe. The most common valence states of Cr in soils and natural waters are Cr(III) and Cr(VI).[2] Under oxic conditions, Cr speciation is dominated by the highly soluble and mobile Cr(VI) species, chromate (CrO_4^{2-}) and bichromate ($HCrO_4^{2-}$).[3] Due to its higher bioavailability and strong oxidizing capability, Cr(VI) exhibits a toxicity threat that is 100 times greater than that of Cr(III).[4] Contrastingly, under circumneutral pH conditions, Cr(III) is traditionally considered insoluble and stable.[3] A wide range of reactants are capable of reducing Cr(VI) to Cr(III), including biotic (e.g., dissimilatory metal reducing microbes)[5−8] and abiotic (e.g., sulfide, Fe(0), Fe(II), and organic compounds)[9−13] pathways. The common reduction products are either pure Cr(III)-(oxy)hydroxides or a mixed Cr(III)-Fe(III)-(oxy)hydroxide solid solution series in the presence of iron (Fe) and due to the structural similarities between Cr(III) and Fe(III).[12,14,15] These (oxy)hydroxides are sparingly soluble[14] and are typically considered as the ultimate sink of Cr in subsurface environments.[2]

Cr(III) can be oxidized by ubiquitous manganese (Mn) oxides to Cr(VI), which leads to contamination.[16] Studies have shown that the oxidation kinetics of Cr(III) by Mn oxides are affected by Cr speciation (e.g., soluble Cr(III) or Cr(III)−organic complex vs solid $Cr(OH)_3$).[16−21] Thus, understanding the potential solubilization mechanisms of Cr(III)-containing solids under environmental conditions and their subsequent oxidation efficiency by Mn oxides is critical for constraining the fate of Cr in the subsurface[22] and evaluating the long-term efficiency of biotic/abiotic Cr(VI) remediation techniques.

Siderophores and small organic acids are both ubiquitous organic molecules produced by a wide range of microorganisms (e.g., bacteria and fungi) and plants[23,24] and are often coexuded.[25,26] Siderophores are organic chelating agents with a high affinity for Fe(III) and can facilitate Fe solubilization and bioavailability from low solubility Fe(III)-containing mineral

Received: October 25, 2016
Revised: February 15, 2017
Accepted: February 20, 2017
Published: February 20, 2017

DOI: 10.1021/acs.est.6b05408
Environ. Sci. Technol. 2017, 51, 3223−3232

phases (e.g., hematite).[27] Siderophores have also been shown to have strong affinities for other trivalent metal cations, such as Cr(III), Mn(III), and Co(III), due to their structural (i.e., coordination) similarity to Fe(III).[28−30] A wide range of common organic acids (e.g., oxalic, citric, fulvic, and humic acids) have been demonstrated to complex with Cr(III).[17,31−33] In fact, measurements on natural waters, including sites with anthropogenic contaminations, revealed concentrations of dissolved Cr(III) above the solubility of $Cr(OH)_3$ in the absence of organic chelating agents, which was suggested to be due to the complexation of Cr(III) with organic molecules.[34−37] Both siderophores (e.g., desferrioxamine B, rhizoferrin, protochelin)[38] and organic acids (e.g., citric acid, ethylenediaminetetraacetic acid, nitrilotriacetic acid)[39] were recently shown to be capable of solubilizing Cr(III) from the pure Cr(III)-(oxy)hydroxide solid phase under environmentally relevant conditions. However, to our knowledge no studies have examined the solubilization of the mixed Cr(III)-Fe(III)-(oxy)hydroxide solid solution series by these common organic molecules, as well as the transformation of the solid phases upon reaction. Interestingly, the coexistence of siderophores and small organic acids can have positive, neutral, or negative effects on trivalent metal oxide dissolution rate, depending on the metal oxide type, siderophore type, and solution conditions.[26,38,40] Such information is missing for the mixed Cr(III)-Fe(III)-(oxy)hydroxide phases.

In this study, we investigated the dissolution of the Cr(III)-Fe(III)-(oxy)hydroxide solid solution series in the presence of a representative siderophore, desferrioxamine B (DFOB), and the common biogenic organic acid, oxalate. The compositional and structural evolutions of the solid phases were also monitored using a suite of complementary spectroscopic and microscopic techniques. Results from this study provide important insights on the long-term stability of Cr remediation products in the presence of microbial activities.

2. MATERIALS AND METHODS

2.1. Synthesis of Cr(III)-Fe(III)-(oxy)hydroxides. Representative samples from the Cr(III)-Fe(III)-(oxy)hydroxide solid solution series, hereafter referred to as $Cr_xFe_{1-x}(OH)_3$, were synthesized following previous procedures[15] with x = 0, 0.2, 0.5, 0.8, and 1. These samples are referred to as Fe10, Cr2Fe8, Cr5Fe5, Cr8Fe2, and Cr10, respectively (Supporting Information (SI) Table S1). Briefly, $Fe(NO_3)_3{\cdot}9H_2O$ and $Cr(NO_3)_3{\cdot}9H_2O$ (both ACS grade) were dissolved in deionized water (18 MΩ cm) to obtain a total metal concentration of 0.1 M with desired Cr(III):Fe(III) molar ratios. The solutions were slowly titrated to pH 7 with 1 M NaOH. Precipitates formed from the suspension were aged for 24 h followed by dialysis to remove remaining electrolytes. The resulting wet pastes were recovered, freeze-dried, and finely ground. Portions of the powders were dissolved in nitric acid for analysis of Cr and Fe compositions by inductively coupled plasma-mass spectroscopy (ICP-MS). Specific surface area of each dried solid was determined by Brunauer−Emmett−Teller (BET) gas adsorption analysis using an Autosorb-1-MP surface pore analyzer (Quantachrome Corp.) (SI Table S1).

2.2. Ligand Solubilization Experiments. Stabilities of the synthesized $Cr_xFe_{1-x}(OH)_3$ solids were investigated in the presence or absence of a representative siderophore, DFOB, and/or a representative small organic acid, oxalate. The solids (0.2 g/L) were suspended in a 0.1 M NaCl electrolyte solution with 10 mM 4-(2-hydroxyethyl)-1-piperazineethanesulfonic acid (HEPES, high purity grade) buffer at pH 7 and sonicated for 15 min. This buffer has been previously shown to not influence the rates of siderophore promoted dissolution of metal hydroxides[25,38,41] After addition of the solid, the suspensions were sonicated for 15 min to disperse particles. For the treatments containing oxalate, oxalic acid (ACS grade) was added to the suspension to achieve a final concentration of 0.1 or 1 mM. For the treatments containing DFOB, a mesylate salt of DFOB (Sigma-Aldrich) was added to the suspensions for a final DFOB concentration of 0.1 mM. For the treatments containing both DFOB and oxalate, oxalic acid was added 1 min prior to DFOB addition in order to account for the potential effect of oxalate on metal hydroxide dissolution during the initial duration of exposure to oxalate.[26] Each treatment was conducted in duplicate in batch reactors in the dark by using amber bottles or by wrapping the reaction bottles in aluminum foil. Reaction bottles were constantly agitated at room temperature on an orbital shaker.

Aliquots of each sample were collected throughout a time series, syringe filtered (0.2 μm, cellulose acetate, VWR), and analyzed for total dissolved Cr and Fe concentrations by ICP-MS. The formation and concentration of Fe(III)−DFOB complex was monitored at 430 nm by UV−visible (UV−vis) spectroscopy (Cary 60, Agilent).[42] Cr(VI) concentration in the filtrates was analyzed using the diphenylcarbazide assay by UV−vis at 540 nm[16] and was below the detection limit for all treatments. Thus, the total dissolved Cr concentration in the filtrate was considered to be Cr(III). The pH value of each suspension stayed at 7.0 ± 0.1 throughout the entire experiment for all treatments. No microbial growth was observed for the duration of the experiment. Release rates were determined by fitting a regression line through the dissolution profile over the same time frame (21 days) for each condition and normalizing to BET surface area of each solid. Additionally, mass normalized dissolution rates are also presented as the BET measured specific surface area of noncrystalline solid phases may be limited by the size of the gas molecule used[43] and underestimated due to increased aggregation[44,45] and surface decomposition during degassing.[46] Uncertainty estimates represent the variance of the rate determined from regression analysis and error from duplicates. At the end of the experiment, the reacted solids were freeze-dried and characterized using X-ray absorption spectroscopy (XAS), pair distribution function (PDF) analysis of X-ray total scattering, and high resolution transmission electron microscopy (HRTEM).

2.3. Synchrotron X-ray Scattering Analysis of Solid Phases. High-energy X-ray total scattering data of both pristine and reacted $Cr_xFe_{1-x}(OH)_3$ samples were collected at beamline 11-ID-B (~58.6 keV, λ = 0.2117 Å) of the Advanced Photon Source (APS), Argonne National Laboratory, IL. Conversion of data from 2D to 1D was performed using the program Fit2D.[47,48] The experimental total scattering structure function $S(Q)$, reduced experimental structure function $f(Q)$, and PDF, or $G(r)$, were obtained using PDFgetX2.[49] Compositions used for the normalization of the experimental structure functions are included in SI Table S1. Since there are currently no detailed structure models for the compositional series, we adopted a self-consistent method assuming the general formula of $(Cr,Fe)_2O_3{\cdot}nH_2O$ for all samples. Information obtained regarding the Fe:Cr ratio of the unreacted solids (from ICP-MS analysis) was incorporated in the compositions used for PDF normalization. Total hydration

DOI: 10.1021/acs.est.6b05408
Environ. Sci. Technol. 2017, 51, 3223−3232

information from thermal gravimetric analysis (TGA) of the weight loss for the unreacted samples[15] was used for estimating the hydration states of all other samples and was incorporated in the normalization. This normalization approach resulted in consistent reduced structure functions for all samples, and the PDFs were calculated from the Fourier transforms of these data truncated at 29 $Å^{-1}$. The size of the coherent scattering domain for each sample was estimated from the attenuation of the PDF as a function of r (Å).

2.4. Synchrotron X-ray Absorption Spectroscopy (XAS) of Solid Phases. Cr and Fe K-edge XAS data were collected for all pristine and reacted samples at beamlines 5-BM-D and 12-BM-B at APS, and beamline 4−1 at Stanford Synchrotron Radiation Lightsource (SSRL), CA. Freeze-dried, finely ground sample powders were evenly brushed on Kapton tapes and excess powders were blown off. Several layers of the sample-loaded tapes were stacked to achieve desired thickness. Depending on Cr or Fe concentrations, X-ray absorption near edge structure (XANES) data were collected either in transmission or fluorescence mode (using a Lytle or Vortex detector depending on beamline setup). Energy calibration used Cr or Fe metal foils. A monochromator detuning of 50% were used for both Cr and Fe K-edges to minimize higher-order harmonics. Data processing was performed with the data analysis programs SIXPack[50] and Ifeffit.[51]

2.5. High Resolution Transmission Electron Microscopy (HRTEM). HRTEM images of both pristine and DFOB-reacted $Cr_xFe_{1-x}(OH)_3$ samples (reaction time of 32 days) were taken on a JEOL 2010F TEM. A small amount of each sample was dispersed in ethanol and ultrasonicated for ~ 1 min. Then, a drop of the suspension was placed onto a 200-mesh Cu grid with a holey-carbon support film and air-dried. To avoid beam damage, image focus was obtained on the carbon film adjacent to the particles of interest, and then the beam was moved onto the sample particle. Due to the small crystal sizes (5 nm and less), the electron diffraction is very weak. Therefore, we used fast Fourier transform (FFT) to appraise the diffraction and crystallinity of each sample.

3. RESULTS AND DISCUSSION

3.1. DFOB and/or Oxalate Mediated Solid Dissolution. In the absence of DFOB and oxalate (i.e., control experiments), dissolved Fe and Cr remained less than 0.5 μM for all $Cr_xFe_{1-x}(OH)_3$ solids throughout the experiments (30−35 days) (Figure 1A). The presence of DFOB and/or oxalate promoted the dissolution of Cr and/or Fe to different extents, as discussed below.

The presence of 0.1 mM DFOB promoted the release of both Fe and Cr from all solid phases as compared to the control experiments, with Fe released at both a higher rate and extent than Cr (Figure 1B). For all experiments, Fe concentrations gradually increased until reaching plateaus after ~ 20 days. At the end of experiments, sample Fe10 released the most Fe into solution (~60 μM), followed by Cr5Fe5 (~30 μM), Cr8Fe2 (~10 μM), and Cr2Fe8 (~5 μM) (Figure 1B). All Fe was released as the Fe(III)−$HDFOB^+$ complex (SI Figure S1) as expected at pH 7.[52] Cr release was slightly promoted in the presence of DFOB as compared to control experiments, with dissolution plateaus reached after ~25 days for all solids except for Cr10, which continued to release Cr through the end of the experiment. At the end of experiments (32 days), Cr10 released the most Cr into solution (~1.5 μM), followed by Cr5Fe5, Cr2Fe8, and Cr8Fe2 (all ~1 μM). No Cr(VI) was detected in

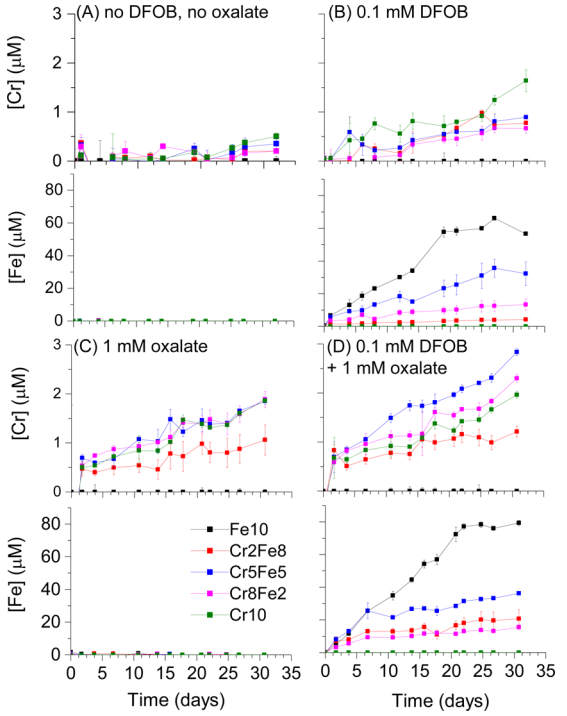

Figure 1. Concentrations of dissolved Cr and Fe from the $Cr_xFe_{1-x}(OH)_3$ phases in the presence of (A) no DFOB, no oxalate (control), (B) 0.1 mM DFOB, (C) 1 mM oxalate, and (D) 0.1 mM DFOB + 1 mM oxalate. Experiments were conducted at pH 7 in 0.1 M NaCl with 0.2 g L^{-1} of each solid.

all experiments. Thus, the total dissolved Cr was considered Cr(III). We were not able to differentiate Cr(III)−DFOB complex from dissolved Cr(III) because there were no observable spectra for the Cr(III)−DFOB complex by UV−vis spectroscopy (200−800 nm). The absence of spectral features is due to the low molar absorptivity coefficient of the Cr(III)-DFOB complex (ε_{max} < 70 L mol^{-1} cm^{-1})[53] and small concentrations present in this study, as has been previously described.[38] However, by comparing Cr(III) release in the control experiments (Figure 1A) and DFOB experiments (Figure 1B), the additional release of Cr(III) in the DFOB experiments can be attributed to the complexation between Cr(III) and DFOB, as DFOB has been previously shown to promote the dissolution of $Cr(OH)_3$ through complexation.[38] The higher dissolution rate and extent for Fe relative to Cr from the solid phases in the presence of DFOB is consistent with the greater stability constant for the Fe(III)−$HDFOB^+$ complex ($10^{32.2}$)[54] relative to that of the Cr(III)-$HDFOB^+$ complex ($10^{30.6}$).[38] In fact, siderophore-promoted dissolution rates have been shown to correlate with the stability constant of the corresponding aqueous metal-siderophore complex.[55] The preferential mobilization of Fe from the solid phases resulted in the enrichment of Cr in the remaining solid phases, which is discussed later. The dissolution rate of the Fe10 endmember (previously described as 2-line ferrihydrite)[15] is consistent with previously reported surface area normalized and mass normalized rates of DFOB-promoted dissolution of ferrihydrite[56] and surface area normalized rates of DFOB-promoted dissolution of goethite,[57,56,58] on the order of 10^{-13} mol $m^{-2}s^{-1}$ and 10^1 μmol $g^{-1}day^{-1}$, at circumneutral pH and similar experimental conditions (SI Tables S2 and S3). When rates are normalized to surface area, the dissolution of goethite is directly

DOI: 10.1021/acs.est.6b05408
Environ. Sci. Technol. 2017, 51, 3223−3232

comparable to that of ferrihydrite.[56] The surface area normalized dissolution rate of the Cr10 endmember is an order of magnitude less than the rate reported by Duckworth et al.[38] This difference in rate may be the result of small differences in experimental conditions and properties of the initial $Cr(OH)_3$ solids.

The effect of oxalate alone on the release of Cr from all solids was dependent on oxalate concentration. The presence of 0.1 mM oxalate did not have a significant impact on Cr release rate and extent (SI Figure S2A), whereas 1 mM oxalate (Figure 1C) not only enhanced the extent of Cr release (up to ∼1−2 μM Cr), but also resulted in continuous increase at 30 days. As a hard acid, Cr(III) forms strong complexes with hard bases, including carboxylate ligands such as oxalate.[59] Oxalate has been shown to adsorb to Cr(III) hydroxide via inner sphere coordination,[60] which is the initial step for ligand promoted surface detachment and dissolution.[61] Citrate has also been shown to dissolve amorphous $Cr(OH)_3$ at pH ∼ 7.[39] Contrastingly, no Fe was released throughout the experimental course in the presence of oxalate alone (Figure 1C and SI Figure S2A), which is consistent with previous studies that showed negligible dissolution of Fe oxides in the presence of oxalate in the circumneutral pH range.[55,62−64]

In the presence of both DFOB (0.1 mM) and oxalate, the addition of 1 mM oxalate increased the release rate of Fe from each solid phase in a synergistic manner (i.e., the rate of dissolution in the presence of both oxalate and DFOB is greater than the sum of each rate) (Figure 2, SI Tables S2 and S3). This synergistic effect of oxalate on DFOB-promoted dissolution has been previously reported for Fe oxides and was attributed to the formation of a kinetically labile Fe-oxalate species at the solid surface followed by rapid ligand exchange with DFOB in solution.[26] While this effect was apparent for Fe release from these mixed solids, it was not observed for Cr release rate (Figure 2, SI Tables S2 and S3), similar to previous observations for Mn and Co oxides.[55] The greater impact of oxalate on DFOB-promoted release of Fe relative to Cr most likely reflects the much lower ligand exchange rate for Cr(III) relative to Fe(III),[65] which may limit the synergistic effects of ligand combinations on dissolution rates.

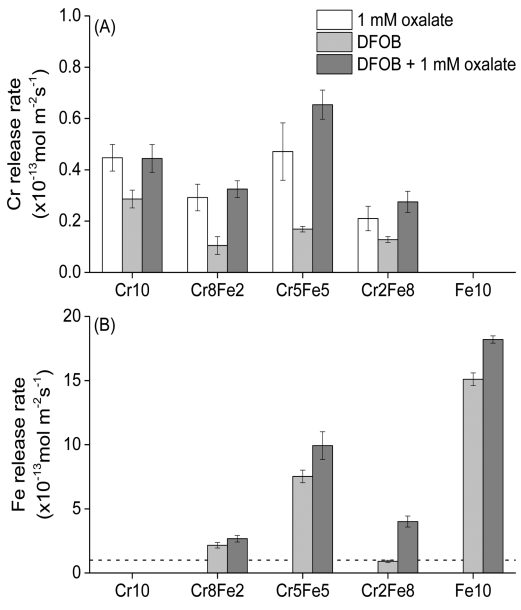

Figure 2. Release rates (mol m^{-2} s^{-1}) of (A) Cr and (B) Fe of each solid phase in the presence of 1 mM oxalate (white), 0.1 mM DFOB (light gray), or 0.1 mM DFOB + 1 mM oxalate (dark gray). Release rates were normalized to surface area of each starting solid and were determined by fitting a regression line through the dissolution profile over the same time frame (∼21 days). Error bars represent variance of the rate determined from regression analysis and error associated with duplicates. The dashed line in (B) is at a release rate of 1 mol $m^{-2}s^{-1}$, which is the maximum value of the *y*-axis in (A).

Interestingly, in the presence of 0.1 mM DFOB and 0.1 mM oxalate, the effect of oxalate addition on DFOB-promoted release of Cr and Fe can be either synergistic, inhibitive, or exhibit no effect on the metal release rates (see SI Text S1). A previous study on the dissolution of Al-substituted goethite phases in the presence of DFOB and oxalate found a similar dependence of Fe release rate on oxalate concentration and solid Al content.[66] Although the reason for such observations is unclear, the combined effect of DFOB and oxalate seems to be affected by oxalate concentration (or DFOB/oxalate ratio) and solid phase composition/structure. It is possible that the exchange between the surface formed labile metal-oxalate sufrface complex and metal-DFOB complex is affected by the ligand exchange rate of each metal ion, and the water exchange rate for Cr(III) is known to be much slower than Fe(III).[65] Higher concentrations of oxalate might facilitate the formation of surface metal−oxalate labile complex and provide more opportunities for metal exchange with DFOB. Furthermore, different concentration ratios of organic acid and siderophore may affect the competition for surface sites, as has been proposed to explain the inhibition of citrate on DFOB-promoted dissolution of Fe oxides.[26,67]

The impact of the $Cr_xFe_{1-x}(OH)_3$ solid composition on the DFOB + oxalate combined effect is likely related to the structural and/or surface properties of these solids. A consistent trend observed throughout our treatments is that both the dissolution rate and extent of Fe and Cr from Cr5Fe5 are greater than those of the other intermediate composition phases, Cr2Fe8 and Cr8Fe2 (Figure 1B−D, SI Table S2). Under all conditions, the rate of Fe release (μmol day^{-1} g^{-1}) is consistent when normalized to Fe content (SI Table S3) for all solids, except for Cr2Fe8, suggesting that perhaps this solid phase behaves inconsistently. Our previous study demonstrated that this nanosized $Cr_xFe_{1-x}(OH)_3$ solid solution series does not follow the structural characteristics of traditional solid solutions of bulk crystalline materials.[15] The Fe10 end member (i.e., 2-line ferrihydrite) is a nanocrystalline phase,[15,68] and the Cr10 end member is truly amorphous.[15] Under HTREM, the loss of lattice fringes and discontinuation of nanocrystallinity seemed to occur between Cr5Fe5 and Cr7Fe3.[15] Therefore, it is possible that such structural/crystallinity change (i.e., different arrangements of surface atoms) and compositional change (e.g., hydration state) can expose different amount and type of Fe and/or Cr sites on the surface for complexation with oxalate and/or DFOB.

3.2. Composition Evolution of Solid Phases. The preferential mobilization of Fe from all solid phases in the presence of DFOB alone or DFOB + oxalate led to the evolution of the solid phases to be more enriched in Cr relative to the initial solid phases (i.e., all solids exhibited an increased Cr/(Cr+Fe) molar ratio after reaction) (Figure 3). The most drastic changes were observed in Cr5Fe5 (30% change in solid Cr/(Cr+Fe) ratio relative to initial composition), followed by Cr8Fe2 (11%) and Cr2Fe8 (7%), all in the presence of DFOB + 1 mM oxalate. Similar to the effects of the microbially

DOI: 10.1021/acs.est.6b05408
Environ. Sci. Technol. 2017, 51, 3223−3232

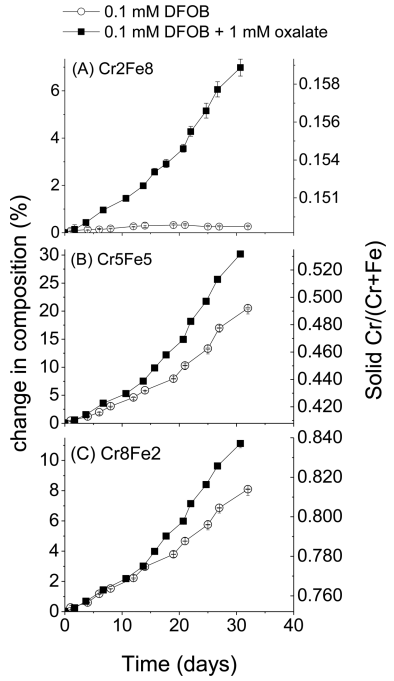

Figure 3. Composition evolution of the of $Cr_xFe_{1-x}(OH)_3$ phases as a function of time in the presence of 0.1 mM DFOB alone or 0.1 mM DFOB + 1 mM oxalate. Change in composition (%) is presented as percent change in solid Cr/(Cr+Fe) molar ratio over time.

produced organic compounds in this study (i.e., siderophores and organic acids), direct microbial activity (e.g., anaerobic respiration of dissimilatory iron reducing bacteria) has also been shown to lead to the evolution of the $Cr_xFe_{1-x}(OH)_3$ phases toward Cr enrichment through the respiration and reduction of Fe(III) within the mixed solid phases.[69] Although the presence of oxalate alone preferentially removed Cr relative to Fe, the composition change of the solid Cr/(Cr+Fe) relative to the initial composition based on this Cr depletion was negligible in all solid phases (<3%).

3.3. Structural Evolution of Solid Phases. The compositional enrichment of Cr in the solid phases was expected to alter the structure of the reacted solid phases relative to the initial solid phases. As previously mentioned, the mixed $Cr_xFe_{1-x}(OH)_3$ phases comprise a nontraditional solid solution series with gradual structural and compositional changes, albeit the two end members have different structures, crystallinity, and chemical compositions.[14,15] The Cr end member exhibits only short-range order with a particle size of ∼10 Å and has a greater hydration state than the Fe end member (2-line ferrihydrite), which exhibits intermediate range order with a coherent domain size of ∼27 Å.[15] In this study, complementary PDF, XAS, and HTREM characterizations were conducted on both the pristine (i.e., initial) and reacted solids to determine (1) whether the reacted solids still have similar structural features as the original solid solution, and if so, (2) where they fall within the solid solution series.

PDF analysis can be used to evaluate coherent domain size and atomic pair correlations of the reacted solids compared to the initial solids. The PDFs of all pristine and reacted solid phases under control (no DFOB, no oxalate) or 0.1 mM DFOB conditions are shown in SI Figure S3. For pristine samples, from Cr10 to Fe10 the PDF spectra show a gradual increase of the coherent domain size with increasing Fe content (SI Figure S3A). The atomic pair correlations of the reacted solids are overall similar to the original solid phases (SI Figure S3B). The prominent feature at ∼2 Å is indicative of the metal−oxygen pair correlation, as both Cr and Fe have similar ionic radii in the +3 valence state. With increasing Cr content, there is a shift of the features at 3 Å (edge-sharing metal-metal octahedra) and 3.4 Å (corner-sharing metal-metal octahedra), indicating gradual structural changes. The coherent domain sizes of reacted samples are slightly larger than those of the pristine samples, possibly due to an aging effect (SI Figure S3A). Interestingly, the solids reacted with DFOB exhibit smaller coherent domain sizes than the respective control experiments, likely due to the partial dissolution promoted by DFOB complexation.

Because PDF is not an element sensitive technique and Cr and Fe have similar scattering properties, Cr and Fe K-edge XAS analyses were conducted to confirm that the increased structure order revealed by PDF was not indicative of the formation of different phase(s) other than the solid solution series. Both Cr and Fe XAS spectra of the ligand-reacted samples showed spectral features similar to those observed within the solid solution series (Figure 4 and SI Figures S4, and S5). As previously observed with the solid solution series,[15] gradual structural transformations were also observed for the reacted samples, as indicated by the vertical lines in Figure 4 and SI Figure S4. No Cr(VI) was observed in any of the samples, as evidenced by the absence of an intense pre-edge peak at ∼ 5989 eV.[70] The weak pre-edge feature at ∼5992 eV is typical of Cr(III)-containing compounds[71] and further confirms that no redox reactions have occurred during the experiments. The Cr XANES spectra of the reacted solids also differ significantly from the reported spectra of most likely products (e.g., Cr-substituted goethite; CrOOH)[72] if a transformation of the local structure had occurred. Moreover, if these crystalline phases indeed formed in our system, they would have showed long-range order in the PDF data of the reacted samples, which was not observed. Thus, the reacted solids had slight increases in crystallinity and structure order (as revealed by PDF) without changes in local coordination environment, similar to ferrihydrite phases with different structure order (e.g., 2-line ferrihydrite vs 6-line ferrihydrite).[73,74]

Representative HRTEM images and FFT analysis further support the change in crystallinity of the solid phases upon reaction (Figure 5). All samples show heavy aggregation, however, in this current study it is not possible to constrain whether the level of aggregation was present in the reaction suspensions or whether more aggregation was induced due to the sample preparation procedure for HRTEM. In general, there is a loss of structural order from Fe10 to Cr10, and the samples reacted with DFOB are less crystalline than the control samples. HRTEM images show that Fe10 and Cr2Fe8 both have clear lattice fringes and the grain sizes are ∼5 nm in both the control and reacted samples. With increasing Cr content (e.g., samples Cr5Fe5, Cr8Fe2, and Cr10), the lattice fringes are only vaguely seen, and amorphous structures dominate the samples. Bright spots can be seen in the FFT patterns of samples Fe10, Cr2Fe8, and Cr5Fe5, reflecting the existence of nanocrystalline structure. However, in samples Cr8Fe2 and Cr10, bright spots are not obvious and only broad diffuse rings are observed. The diffuse rings also broaden from Cr8Fe2 to Cr10, which is consistent with the disappearance of lattice fringes and decrease of structural order.

DOI: 10.1021/acs.est.6b05408
Environ. Sci. Technol. 2017, 51, 3223−3232

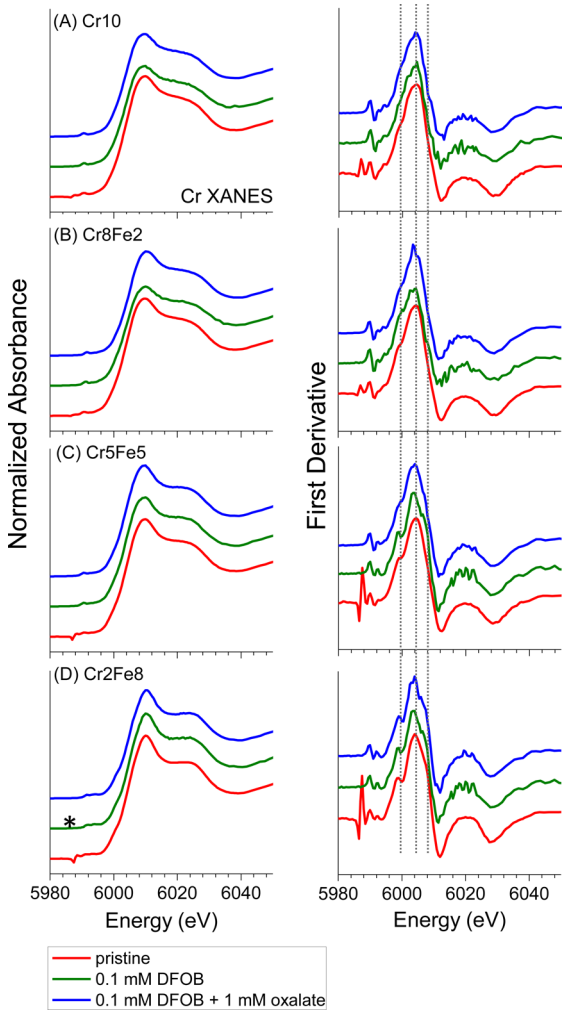

Figure 4. Cr K-edge XANES spectra (left) and corresponding first derivatives (right) of (A) Cr10, (B) Cr8Fe2, (C) Cr5Fe5, and (D) Cr2Fe8 under pristine, control, 0.1 mM DFOB alone, and 0.1 mM DFOB + 1 mM oxalate conditions. Vertical lines indicate regions where gradual transformations are observed. The sharp feature at ~5985 eV present in the pristine samples (indicated by the asterisk) is a monochromator glitch.

Taken together, solid phase analyses reveal that the reacted solids belong to the same solid solution series, with each reacted solid having higher Cr content and a structure representative of Cr enrichment. However, because of the relatively small compositional changes (<10% of the overall solid Cr/(Cr+Fe) mole ratio, Figure 3), the changes are subtle in XAS and HRTEM analyses.

3.4. Incongruent Dissolution of the Solid Phases. Based on the observed structural changes, dissolution requires some mechanism to induce changes in the local coordination environment of Cr and Fe. The dissolution mechanism itself is not straightforward because these mixed solids represent a nontraditional solid solution where the structures of the end members are not the same, and there is a gradual change in the structure along the compositional series.[15] For solid phases containing both Cr and Fe (i.e., Cr2Fe8, Cr5Fe5, Cr8Fe2), regardless of ligand type and concentration, the release (both rate and extent) of Cr and Fe are not proportional to their molar ratio in the solid [i.e., $x/(1-x)$]. Therefore, the overall dissolution is incongruent and produces a secondary solid phase with compositions different from the unreacted solid. In the presence of DFOB alone or DFOB + oxalate, the produced

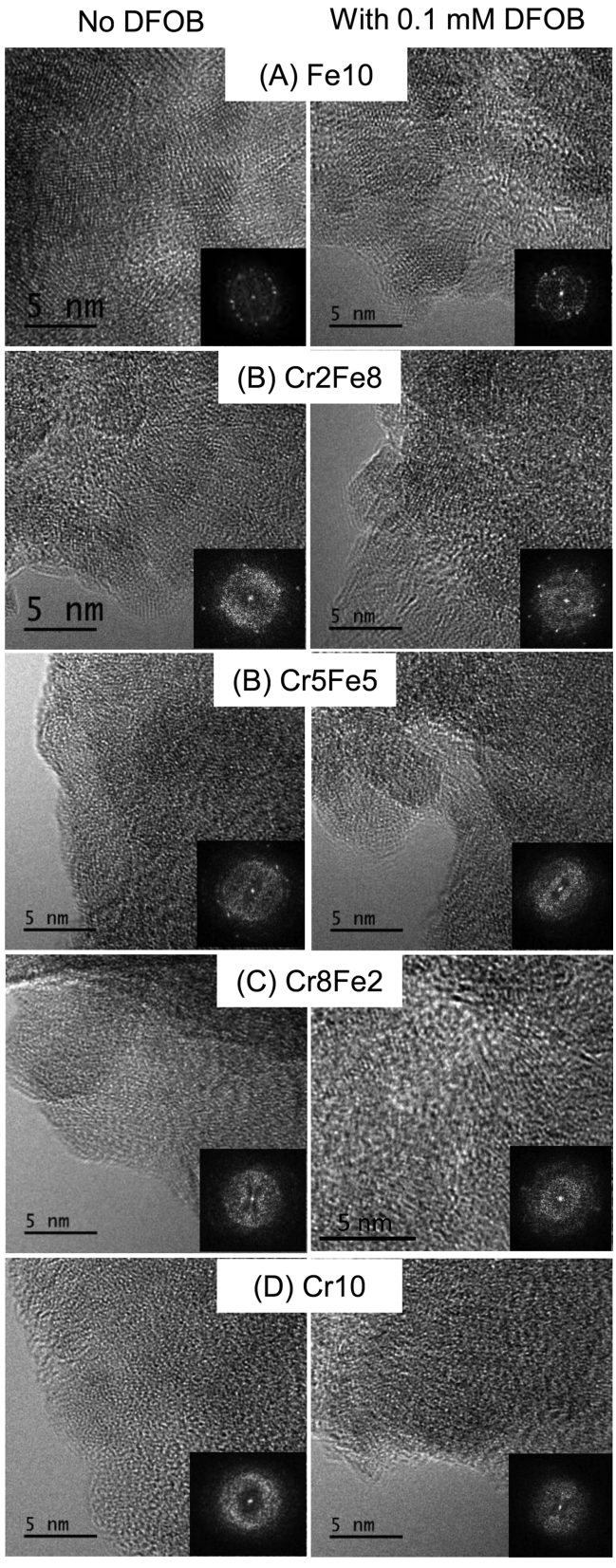

Figure 5. HRTEM images and corresponding FFT patterns of reacted (32 days) solid phases under control (left panels) or 0.1 mM DFOB (right panels) conditions. Scale bars are 5 nm.

DOI: 10.1021/acs.est.6b05408
Environ. Sci. Technol. 2017, 51, 3223−3232

secondary solid phase is more enriched in Cr. In the presence of oxalate alone, the preferential release of Cr (but not Fe) from these solids results in the slight enrichment of Fe. Incongruent dissolution of traditional solid solution series is typically discussed in the context of geological weathering. For example, previous studies showed that in the presence of oxalate, Al and Ca were preferentially removed (relative to Si) from feldspars,[75,76] resulting in a leached layer depleted in Al and Ca on the mineral surface.[77] A leached layer is defined as a chemically altered zone at the solid-solution interface, which exhibits a different elemental composition than the bulk solid composition.[78,79] The most likely mechanism leading to the observed structural changes in our system can occur from the structural reconstruction of this leached layer to minimize the surface energy configuration as has been observed in silicate minerals.[78] In the case of a leached layer, the preferential dissolution of Fe would result in a Cr enriched leached layer, which may spontaneously reconstruct to form a structure that would be identical to the solid phase initially precipitated with the corresponding Cr/Fe ratio. Because of the nanoscale size of the $Cr_xFe_{1-x}(OH)_3$ primary particles (i.e., 1−2 nm as identified by PDF) and associated large surface:bulk ratio, the reorganization of the surface is more evident as the overall transformations observed in the XAS and HRTEM analyses.

4. ENVIRONMENTAL IMPLICATIONS

Understanding the potential reaction kinetics and pathways of Cr(VI) remediation products in the presence of microbial activities and/or metabolites has significant implications for assessing their long-term stability under natural conditions. In this study, we investigated the single and combined effects of a siderophore, DFOB, and an organic acid, oxalate, on the stability of the Cr(III)-Fe(III)-(oxy)hydroxide solid solution series. Siderophores and organic acids are both common microbial exudates in the natural environments. Our study reveals that Cr(VI) remediation products may be remobilized in the subsurface by these common microbially secreted ligands via (1) the direct ligand-promoted solubilization of Cr(III) from the Cr(III)-Fe(III)-(oxy)hydroxide solid phases, as well as (2) increased solubility of the secondary solid phases resulted from incongruent dissolution of the starting solid phases, as discussed below.

(1) Ligand promoted solubilization. The presence of DFOB and/or oxalate led to enhanced release of Cr(III) from the solid phases as a ligand complexed species (Figure 1). Thus, Cr mobility is expected to be promoted in the presence of environmentally relevant organic compounds. Oxalic acid is abundant in soils with concentrations on the order of 10^{-5} to 10^{-3} M range.[80] DFOB is a trihydroxamate siderophore produced by bacteria and fungi under low Fe availability conditions to solubilize Fe(III) from its low solubility (oxyhydr)oxide forms.[56,81] Although the average concentration ranges of siderophores in soil and sediment environments are typically low and difficult to detect (e.g., hydroxamate siderophores in soils typically range from 10^{-8} to 10^{-7} M),[81] the concentration of siderophores can be highly concentrated locally to facilitate the dissolution and mobilization of Fe from the Cr(III)-Fe(III)-(oxy)-hydroxide and consequently mobilize Cr(III) at the same time.[82]

(2) Increased solubility of the secondary solid phases produced by incongruent dissolution of the starting solid phases. As previously discussed, the incongruent dissolution of the initial solids produces secondary solid phases with different composition and structure within the $Cr_xFe_{1-x}(OH)_3$ solid solution series. In the presence of DFOB alone or DFOB + oxalate, the secondary solid phases have higher mole fraction of Cr (x) and are predicted to be more soluble than the starting solids (Figure 6, SI Table S4) based on the data from Sass and Rai[14] and equation derived in Rai et al.:[83]

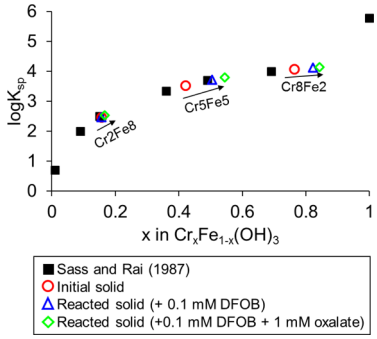

Figure 6. Predicted K_{sp} changes in the reacted $Cr_xFe_{1-x}(OH)_3$ solids in the presence of DFOB alone or DFOB + oxalate as compared to the initial solids, using calculated K_{sp} values and relationship from Sass and Rai[14] and given by the equation $\log K_{CrxFe1-x(OH)3} = 4.23 - 0.172(1-x)^2 - 1.392(1-x)^3 + \log x$ for $0 < x < 0.9$.[83]

$$\log K_{Cr_xFe_{1-x}(OH)_3} = 4.23 - 0.172(1-x)^2 - 1.392(1-x)^3 + \log x$$

(where x = 0 to 1) This equation describes the solubility product (K_{sp}) of each solid phase within the solid solution series as a function of the mole fraction of Cr (and Fe). Based on this equation, the calculated solubility product of the secondary solid phases increased by ~0.1 to 9% in the presence of DFOB (SI Table S4). Such increased solubility can lead to increased opportunity for the oxidation of Cr(III) to the toxic Cr(VI). Ligand-promoted dissolution leading to increased solubility of the remaining solid phase has previously been observed in hausmannite ($Mn^{2+}Mn^{3+}{}_2O_4$).[84] During DFOB-promoted dissolution of hausmannite, the depletion of Mn(III) from the solid phase led to structural instability that induced dissolution of the remaining solids and release of Mn(II).

The above-mentioned processes both produce soluble Cr(III) species (i.e., dissolved or ligand-complexed) that may be more susceptible to reoxidation to Cr(VI) than the solid phase species, leading to subsequent recontamination. Mn oxides are the most dominant environmentally relevant oxidants for Cr(III).[12,16,85] Several studies have examined the oxidation of dissolved Cr(III) by Mn oxides.[86−89] Studies have also shown that the oxidation of Cr(III) bounded by organic ligands, while kinetically slower than inorganic aqueous Cr(III), is a viable mechanism for Cr(III) oxidation to Cr(VI).[21,90]

Under complex environmental conditions, besides the above-mentioned processes (e.g., dissolution of Cr-containing solids, production of dissolved Cr(III) and/or Cr(III)−ligand complex, oxidation of dissolved Cr(III) ion or Cr(III)-ligand complex by Mn oxides), other biogeochemical processes and

DOI: 10.1021/acs.est.6b05408
Environ. Sci. Technol. 2017, 51, 3223−3232

factors should also be taken into consideration to better constrain the ultimate fate of Cr and its remediation byproducts. Organic ligands might interact with Mn oxides and influence their oxidation efficiency. For example, at circumneutral pH, DFOB has been shown to dissolve Mn oxides, either through reductive dissolution (leading to the degradation of DFOB and production of aqueous Mn(II)) or ligand complexation (leading to Mn(III)−DFOB complex formation).[91] The presence of oxalate can promote and enhance the reductive dissolution pathway.[40] The DFOB-promoted dissolution rates of Mn oxides under experimental conditions similar to this study are 10^{-9} mol m^{-2} s^{-1}.[55] Therefore, the interaction between organic ligands and Mn oxides may be a kinetically competitive process to the ligand-promoted dissolution of $Cr_xFe_{1-x}(OH)_3$ solids and subsequently reduce the opportunity for Cr mobilization.

Although our study was only conducted at the environmentally relevant pH value of 7, previously described trends can help provide implications for other pH values. For example, at lower pH values, proton-promoted dissolution of the solid phases becomes more dominant.[38] However, this process is expected to have a similar effect as siderophores on the dissolution kinetics of the solid phases with different compositions, because proton-promoted dissolution rates correlate to the water exchange rates of the cation.[92] Therefore, Fe is expected to preferentially release from the solid phases relative to Cr at lower pH values. At higher pH values, ligand promoted dissolution is the dominant dissolution mechanism and, in general, the rate may increase with increasing pH values.[38] Furthermore, the organic acid and siderophore choice made in this study can help provide insights for other ligands. For example, DFOB as a trihydroxamate siderophore may have a weaker effect than catecholate siderophores and, thus, is expected to result in lower dissolution rates than catecholate siderophores.[38,55] Additionally, the synergistic effect of oxalate may be higher than that of other organic acids.[26] Overall, in mixed metal solid phases, the water exchange rate and metal coordination environment are important factors in predicting the stability and transformation products of solids in the presence of microbial activities.

■ ASSOCIATED CONTENT

Supporting Information

The Supporting Information is available free of charge on the ACS Publications website at DOI: 10.1021/acs.est.6b05408.

Results and discussion for experimental treatments with 0.1 mM oxalate and 0.1 mM DFOB; sample information; initial Fe and Cr release rates; calculated logK_{sp} values for reacted solids; dissolution profile of Fe(III), [Fe(III)-HDFOB]$^+$ complex, and Cr(III); PDF data of pristine and reacted solids; Fe K-edge XANES and corresponding 1st derivatives of pristine and reacted solids; Fe and Cr K-edge XANES and corresponding 1st derivatives of control solids (PDF)

■ AUTHOR INFORMATION

Corresponding Author

*Phone: 404-894-3814; e-mail: yuanzhi.tang@eas.gatech.edu

ORCID

Yuanzhi Tang: 0000-0002-7741-8646

Notes

The authors declare no competing financial interest.

■ ACKNOWLEDGMENTS

This project is support by NASA Astrobiology Institute under Cooperative Agreement No. NNA15BB03A and NASA Exobiology NNX16AL06G. We thank Tyler Sowers and Dr. Dean Hesterberg for help with BET surface area measurements. Portions of this research were conducted at the Stanford Synchrotron Radiation Lightsource (SSRL) and the Advanced Photon Source (APS). SSRL is a Directorate of SLAC National Accelerator Laboratory and an Office of Science User Facility operated for the U.S. Department of Energy Office of Science by Stanford University. APS is a U.S. Department of Energy (DOE) Office of Science User Facility operated for the DOE Office of Science by Argonne National Laboratory under Contract No. DE-AC02-06CH11357. We acknowledge beamline scientists Qing Ma (APS 5-BM-D), Sungsik Lee (APS 12-BM-B), and Ryan Davis (SSRL 4-1) for assistance with experimental set up and data collection.

■ REFERENCES

(1) U. S. EPA. Office of Research and Development. *In situ* treatment of soil and groundwater contaminated with chromium. EPA/625/R-00/005, October 2000.

(2) Richard, F. C.; Bourg, A. C. M. Aqueous geochemistry of chromium: A review. *Water Res.* **1991**, *25* (7), 807−816.

(3) Rai, D.; Eary, L. E.; Zachara, J. M. Environmental chemistry of chromium. *Sci. Total Environ.* **1989**, *86* (1−2), 15−23.

(4) Norseth, T. The carcinogenicity of chromium. *Environ. Health Perspect.* **1981**, *40*, 121−130.

(5) Lovley, D. R.; Phillips, E. J. P. Reduction of chromate by *Desulfovibrio vulgaris* and its c_3 cytochrome. *Appl. Environ. Microbiol.* **1994**, *60* (2), 726−728.

(6) Tebo, B. M.; Obraztsova, A. Y. Sulfate-reducing bacterium grows with Cr(VI), U(VI), Mn(IV), and Fe(III) as electron acceptors. *FEMS Microbiol. Lett.* **1998**, *162* (1), 193−198.

(7) Francis, C. A.; Obraztsova, A. Y.; Tebo, B. M. Dissimilatory metal reduction by the facultative anaerobe *Pantoea agglomerans* SP1. *Appl. Environ. Microbiol.* **2000**, *66* (2), 543−548.

(8) Fredrickson, J. K.; Kostandarithes, H. M.; Li, S. W.; Plymale, A. E.; Daly, M. J. Reduction of Fe(III), Cr(VI), U(VI), and Tc(VII) by *Deinococcus radiodurans* R1. *Appl. Environ. Microbiol.* **2000**, *66* (5), 2006−2011.

(9) Pettine, M.; Millero, F. J.; Passino, R. Reduction of chromium (VI) with hydrogen sulfide in NaCl media. *Mar. Chem.* **1994**, *46* (4), 335−344.

(10) Pettine, M.; D'Ottone, L.; Campanella, L.; Millero, F. J.; Passino, R. The reduction of chromium (VI) by iron (II) in aqueous solutions. *Geochim. Cosmochim. Acta* **1998**, *62* (9), 1509−1519.

(11) Deng, B. L.; Stone, A. T. Surface-catalyzed chromium(VI) reduction: Reactivity comparisons of different organic reductants and different oxide surfaces. *Environ. Sci. Technol.* **1996**, *30* (8), 2484−2494.

(12) Eary, L. E.; Rai, D. Chromate removal from aqueous wastes by reduction with ferrous iron. *Environ. Sci. Technol.* **1988**, *22* (8), 972−977.

(13) Wittbrodt, P. R.; Palmer, C. D. Reduction of Cr(VI) in the presence of excess soil fulvic acid. *Environ. Sci. Technol.* **1995**, *29* (1), 255−263.

(14) Sass, B. M.; Rai, D. Solubility of amorphous chromium(III)-iron(III) hydroxide solid solutions. *Inorg. Chem.* **1987**, *26* (14), 2228−2232.

(15) Tang, Y. Z.; Michel, F. M.; Zhang, L. H.; Harrington, R.; Parise, J. B.; Reeder, R. J. Structural properties of the Cr(III)-Fe(III) (oxy)hydroxide compositional series: Insights for a nanomaterial "Solid Solution". *Chem. Mater.* **2010**, *22* (12), 3589−3598.

(16) Bartlett, R.; James, B. Behavior of chromium in soils. 3. Oxidation. *J. Environ. Qual.* **1979**, *8* (1), 31−35.

DOI: 10.1021/acs.est.6b05408
Environ. Sci. Technol. 2017, 51, 3223−3232

(17) James, B. R.; Bartlett, R. J. Behavior of chromium in soils. 5. Fate of organically complexed Cr(III) added to soil. *J. Environ. Qual.* **1983**, *12* (2), 169−172.
(18) Fendorf, S. E. Surface-reactions of chromium in soils and waters. *Geoderma* **1995**, *67* (1−2), 55−71.
(19) Carbonaro, R. F.; Stone, A. T. Oxidation of Cr(III) aminocarboxylate complexes by hydrous manganese oxide: products and time course behaviour. *Environ. Chem.* **2015**, *12* (1), 33−51.
(20) Namgung, S.; Kwon, M. J.; Qafoku, N. P.; Lee, G. $Cr(OH)_3(s)$ oxidation induced by surface catalyzed Mn(II) oxidation. *Environ. Sci. Technol.* **2014**, *48* (18), 10760−10768.
(21) Yang, F.; Guo, J.; Dai, R. N.; Lan, Y. Q. Oxidation of Cr(III)-citrate/tartrate complexes by delta-MnO_2: Production of Cr(VI) and its impact factors. *Geoderma* **2014**, *213*, 10−14.
(22) Papassiopi, N.; Pinakidou, F.; Katsikini, M.; Antipas, G. S. E.; Christou, C.; Xenidis, A.; Paloura, E. C. A XAFS study of plain and composite iron(III) and chromium(III) hydroxides. *Chemosphere* **2014**, *111*, 169−176.
(23) Gadd, G. M. Bioremedial potential of microbial mechanisms of metal mobilization and immobilization. *Curr. Opin. Biotechnol.* **2000**, *11* (3), 271−279.
(24) Ahmed, E.; Holmstrom, S. J. M. Siderophores in environmental research: Roles and applications. *Microb. Biotechnol.* **2014**, *7* (3), 196−208.
(25) Cheah, S. F.; Kraemer, S. M.; Cervini-Silva, J.; Sposito, G. Steady-state dissolution kinetics of goethite in the presence of desferrioxamine B and oxalate ligands: Implications for the microbial acquisition of iron. *Chem. Geol.* **2003**, *198* (1−2), 63−75.
(26) Reichard, P. U.; Kretzschmar, R.; Kraemer, S. M. Dissolution mechanisms of goethite in the presence of siderophores and organic acids. *Geochim. Cosmochim. Acta* **2007**, *71* (23), 5635−5650.
(27) Neilands, J. B. Siderophores: Structure and function of microbial iron transport compounds. *J. Biol. Chem.* **1995**, *270* (45), 26723−26726.
(28) Budzikiewicz, H.; Georgias, H.; Taraz, K. Diastereomeric pyoverdin-chromium(III) complexes. *Z. Naturforsch., C: J. Biosci.* **2002**, *57* (9−10), 954−956.
(29) Parker, D. L.; Sposito, G.; Tebo, B. M. Manganese(III) binding to a pyoverdine siderophore produced by a manganese(II)-oxidizing bacterium. *Geochim. Cosmochim. Acta* **2004**, *68* (23), 4809−4820.
(30) Duckworth, O. W.; Bargar, J. R.; Jarzecki, A. A.; Oyerinde, O.; Spiro, T. G.; Sposito, G. The exceptionally stable cobalt(III)-desferrioxamine B complex. *Mar. Chem.* **2009**, *113* (1−2), 114−122.
(31) Srivastava, S.; Prakash, S.; Srivastava, M. M. Chromium mobilization and plant availability - The impact of organic complexing ligands. *Plant Soil* **1999**, *212* (2), 203−208.
(32) Walsh, A. R.; Ohalloran, J. Chromium speciation in tannery effluent. 1. An assessment of techniques and the role of organic Cr(III) complexes. *Water Res.* **1996**, *30* (10), 2393−2400.
(33) Gustafsson, J. P.; Persson, I.; Oromieh, A. G.; van Schaik, J. W. J.; Sjostedt, C.; Kleja, D. B. Chromium(III) complexation to natural organic matter: Mechanisms and modeling. *Environ. Sci. Technol.* **2014**, *48* (3), 1753−1761.
(34) Nakayama, E.; Tokoro, H.; Kuwamoto, T.; Fujinaga, T. Dissolved state of chromium in seawater. *Nature* **1981**, *290* (5809), 768−770.
(35) Ahern, F.; Eckert, J. M.; Payne, N. C.; Williams, K. L. Speciation of chromium in sea water. *Anal. Chim. Acta* **1985**, *175* (SEP), 147−151.
(36) Kaczynski, S. E.; Kieber, R. J. Hydrophobic C18 bound organic complexes of chromium and their potential impact on the geochemistry of Cr in natural waters. *Environ. Sci. Technol.* **1994**, *28* (5), 799−804.
(37) Icopini, G. A.; Long, D. T. Speciation of aqueous chromium by use of solid-phase extractions in the field. *Environ. Sci. Technol.* **2002**, *36* (13), 2994−2999.
(38) Duckworth, O. W.; Akafia, M. M.; Andrews, M. Y.; Bargar, J. R. Siderophore-promoted dissolution of chromium from hydroxide minerals. *Environ. Sci.-Process Impacts* **2014**, *16* (6), 1348−1359.
(39) Carbonaro, R. F.; Gray, B. N.; Whitehead, C. F.; Stone, A. T. Carboxylate-containing chelating agent interactions with amorphous chromium hydroxide: Adsorption and dissolution. *Geochim. Cosmochim. Acta* **2008**, *72* (13), 3241−3257.
(40) Saal, L. B.; Duckworth, O. W. Synergistic Dissolution of manganese oxides as promoted by siderophores and small organic acids. *Soil Sci. Soc. Am. J.* **2010**, *74* (6), 2021−2031.
(41) Bi, Y. Q.; Hesterberg, D. L.; Duckworth, O. W. Siderophore-promoted dissolution of cobalt from hydroxide minerals. *Geochim. Cosmochim. Acta* **2010**, *74* (10), 2915−2925.
(42) Albrecht-Gary, A. M.; Crumbliss, A. L. Coordination chemistry of siderophores: Thermodynamics and kinetics of iron chelation and release. *Metal Ions in Biological Systems, Vol 35* **1998**, *35*, 239−327.
(43) Brunauer, S.; Emmett, P. H.; Teller, E. Adsorption of gases in multimolecular layers. *J. Am. Chem. Soc.* **1938**, *60*, 309−319.
(44) Anschutz, A. J.; Penn, R. L. Reduction of crystalline iron(III) oxyhydroxides using hydroquinone: Influence of phase and particle size. *Geochem. Trans.* **2005**, *6* (3), 60−66.
(45) Villalobos, M.; Antelo, J. A unified surface structural model for ferrihydrite: Proton charge, electrolute binding, and arsenate adsorption. *Revista Internacional De Contaminacion Ambiental* **2011**, *27* (2), 139−151.
(46) Davis, J. A.; Leckie, J. O. Surface ionization and complexation at oxide-water interface. 2. Surface properties of amorphous iron oxyhydroxide and adsorption of metal ions. *J. Colloid Interface Sci.* **1978**, *67* (1), 90−107.
(47) Hammersley, A. P.; Svensson, S. O.; Hanfland, M.; Fitch, A. N.; Hausermann, D. Two-dimensional detector software: From real detector to idealised image or two-theta scan. *High Pressure Res.* **1996**, *14* (4−6), 235−248.
(48) Hammersley, A. P. *ESRF98HA01T*; ESRF Internal Report, 1998.
(49) Qiu, X.; Thompson, J. W.; Billinge, S. J. L. PDFgetX2: a GUI-driven program to obtain the pair distribution function from X-ray powder diffraction data. *J. Appl. Crystallogr.* **2004**, *37* (4), 678.
(50) Webb, S. M. SIXpack: A graphical user interface for XAS analysis using IFEFFIT. *Phys. Scr.* **2005**, *T115*, 1011−1014.
(51) Ravel, B.; Newville, M. ATHENA, ARTEMIS, HEPHAESTUS: Data analysis for X-ray absorption spectroscopy using IFEFFIT. *J. Synchrotron Radiat.* **2005**, *12*, 537−541.
(52) Martell, A. E.; Smith, R. M.; Motekaitis, R. J. *Critically Selected Stability Constants of Metal Complexes Database Version 5.0*; Texas A & M University: College station: TX, 1998.
(53) Leong, J.; Raymond, N. Coordination isomers of biological iron transport compounds. 4. Geometrical isomers of chromic desferrioxamine-B. *J. Am. Chem. Soc.* **1975**, *97* (2), 293−296.
(54) Martell, A. E.; Smith, R. M. *Critical Stability Constant Database*; National Institute of Science and Technology (NIST): Gaithersburg, MD, 2003.
(55) Akafia, M. M.; Harrington, J. M.; Bargar, J. R.; Duckworth, O. W. Metal oxyhydroxide dissolution as promoted by structurally diverse siderophores and oxalate. *Geochim. Cosmochim. Acta* **2014**, *141*, 258−269.
(56) Neubauer, U.; Furrer, G.; Schulin, R. Heavy metal sorption on soil minerals affected by the siderophore desferrioxamine B: The role of Fe(III) (hydr)oxides and dissolved Fe(III). *Eur. J. Soil Sci.* **2002**, *53* (1), 45−55.
(57) Wolff-Boenisch, D.; Traina, S. J. The effect of desferrioxamine B, enterobactin, oxalic acid, and Na-alginate on the dissolution of uranyl-treated goethite at pH 6 and 25 degrees C. *Chem. Geol.* **2007**, *243* (3−4), 357−368.
(58) Kraemer, S. M.; Cheah, S. F.; Zapf, R.; Xu, J. D.; Raymond, K. N.; Sposito, G. Effect of hydroxamate siderophores on Fe release and Pb(II) adsorption by goethite. *Geochim. Cosmochim. Acta* **1999**, *63* (19−20), 3003−3008.
(59) Pearson, R. G. Hard and soft acids and bases. *J. Am. Chem. Soc.* **1963**, *85* (22), 3533−3539.
(60) Degenhardt, J.; McQuillan, A. J. Mechanism of oxalate ion adsorption on chromium oxide-hydroxide from pH dependence and

DOI: 10.1021/acs.est.6b05408
Environ. Sci. Technol. 2017, 51, 3223−3232

time evolution of ATR-IR spectra. *Chem. Phys. Lett.* **1999**, *311* (3−4), 179−184.
(61) Loring, J. S.; Simanova, A. A.; Persson, P. Molecular scale study of the synergism between oxalate and desferrioxamine-B on goethite dissolution. *Geochim. Cosmochim. Acta* **2007**, *71* (15), A596−A596.
(62) Loring, J. S.; Simanova, A. A.; Persson, P. Highly mobile iron pool from a dissolution-readsorption process. *Langmuir* **2008**, *24* (14), 7054−7057.
(63) Kraemer, S. M. Iron oxide dissolution and solubility in the presence of siderophores. *Aquat. Sci.* **2004**, *66* (1), 3−18.
(64) Eick, M. J.; Peak, J. D.; Brady, W. D. The effect of oxyanions on the oxalate-promoted dissolution of goethite. *Soil Sci. Soc. Am. J.* **1999**, *63* (5), 1133−1141.
(65) Richens, D. T., *The Chemistry of Aqua Ions*; Wiley: Chichester, U.K., 1997.
(66) Cervini-Silva, J.; Sposito, G. Steady-state dissolution kinetics of aluminum-goethite in the presence of desferrioxamine-B and oxalate ligands. *Environ. Sci. Technol.* **2002**, *36* (3), 337−342.
(67) Bondietti, G.; Sinniger, J.; Stumm, W. The reactivity of Fe(III) (hydr)oxides- Effects of ligands in inhibiting the dissolution. *Colloids Surf., A* **1993**, *79* (2−3), 157−167.
(68) Michel, F. M.; Ehm, L.; Antao, S. M.; Lee, P. L.; Chupas, P. J.; Liu, G.; Strongin, D. R.; Schoonen, M. A. A.; Phillips, B. L.; Parise, J. B. The structure of ferrihydrite, a nanocrystalline material. *Science* **2007**, *316* (5832), 1726−1729.
(69) Hansel, C. M.; Wielinga, B. W.; Fendorf, S. R. Structural and compositional evolution of Cr/Fe solids after indirect chromate reduction by dissimilatory iron-reducing bacteria. *Geochim. Cosmochim. Acta* **2003**, *67* (3), 401−412.
(70) Brown, G. E.; Calas, G.; Waychunas, G. A.; Petiau, J. X-Ray absorptions sepctroscopy and its application in mineralogy and geochemistry. *Rev. Mineral.* **1988**, *18*, 431−512.
(71) Peterson, M. L.; Brown, G. E.; Parks, G. A. Direct XAFS evidence for heterogeneous redox reaction at the aqueous chromium/magnetite interface. *Colloids Surf., A* **1996**, *107*, 77−88.
(72) Frommer, J.; Nachtegaal, M.; Czekaj, I.; Kretzschmar, R. The Cr X-ray absorption K-edge structure of poorly crystalline Fe(III)-Cr(III)-oxyhydroxides. *Am. Mineral.* **2010**, *95* (8−9), 1202−1213.
(73) Michel, F. M.; Ehm, L.; Liu, G.; Han, W. Q.; Antao, S. M.; Chupas, P. J.; Lee, P. L.; Knorr, K.; Eulert, H.; Kim, J.; Grey, C. P.; Celestian, A. J.; Gillow, J.; Schoonen, M. A. A.; Strongin, D. R.; Parise, J. B. Similarities in 2- and 6-Line ferrihydrite based on pair distribution function analysis of X-ray total scattering. *Chem. Mater.* **2007**, *19* (6), 1489−1496.
(74) Kukkadapu, R. K.; Zachara, J. M.; Fredrickson, J. K.; Smith, S. C.; Dohnalkova, A. C.; Russell, C. K. Transformation of 2-line ferrihydrite to 6-line ferrihydrite under oxic and anoxic conditions. *Am. Mineral.* **2003**, *88* (11−12), 1903−1914.
(75) Chou, L.; Wollast, R. Study of the weathering of albite at room-temperature and pressure with a fluidized-bed reactor. *Geochim. Cosmochim. Acta* **1984**, *48* (11), 2205−2217.
(76) Holdren, G. R.; Speyer, P. M. pH dependent changes in the rates and stoichiometry of dissolution of an alakali feldspar at room-temperature. *Am. J. Sci.* **1985**, *285* (10), 994−1026.
(77) Shotyk, W.; Nesbitt, H. W. Incongruent and congruent dissolution of plagioclase feldspar: effect of feldspar composition and ligand complexation. *Geoderma* **1992**, *55* (1−2), 55−78.
(78) Casey, W. H.; Westrich, H. R.; Banfield, J. F.; Ferruzzi, G.; Arnold, G. W. Leaching and reconstruction at the surfaces of dissolving chain-silicate minerals. *Nature* **1993**, *366* (6452), 253−256.
(79) Brantley, L. S., Kinetics of Mineral Dissolution. In *Kinetics of Water-Rock Interaction*; Brantley, L. S., Kubicki, D. J., White, F. A., Eds.; Springer New York: New York, NY, 2008; pp 151-210.
(80) Fox, T. R.; Comerford, N. B. Low-molecular-weight organic-acids in selected forest soils of the southeastern USA. *Soil Sci. Soc. Am. J.* **1990**, *54* (4), 1139−1144.
(81) Powell, P. E.; Cline, G. R.; Reid, C. P. P.; Szaniszlo, P. J. Occurrence of hydroxamate siderophore iron chelators in soils. *Nature* **1980**, *287* (5785), 833−834.
(82) Winkelmann, G. Microbial siderophore-mediated transport. *Biochem. Soc. Trans.* **2002**, *30*, 691−696.
(83) Rai, D.; Zachara, J. M.; Eary, L. E.; Girvin, D. C.; Moore, D. A.; Retsch, C. T.; Sass, B. M.; Schmidt, R. L. *Geochemical Behavior of Chromium Species*; Electric Power Research Institute, 1986.
(84) Pena, J.; Duckworth, O. W.; Bargar, J. R.; Sposito, G. Dissolution of hausmannite (Mn_3O_4) in the presence of the trihydroxamate siderophore desferrioxamine B. *Geochim. Cosmochim. Acta* **2007**, *71* (23), 5661−5671.
(85) Amacher, M. C.; Baker, D. E., Redox reactions involving chromium, plutonium, and manganese in soils. In *Resources*; Las Vegas, Nevada, **1982**; p 166.10.2172/5030864
(86) Fendorf, S. E.; Zasoski, R. J. Chromium(III) oxidation by delta-MnO_2.. 1. Characterization. *Environ. Sci. Technol.* **1992**, *26* (1), 79−85.
(87) Tang, Y. Z.; Webb, S. M.; Estes, E. R.; Hansel, C. M. Chromium(III) oxidation by biogenic manganese oxides with varying structural ripening. *Environ. Sci.-Process Impacts* **2014**, *16* (9), 2127−2136.
(88) Landrot, G.; Ginder-Vogel, M.; Livi, K.; Fitts, J. P.; Sparks, D. L. Chromium(III) oxidation by three poorly-crystalline manganese(IV) oxides. 1. Chromium(III)-oxidizing capacity. *Environ. Sci. Technol.* **2012**, *46* (21), 11594−11600.
(89) Kim, J. G.; Dixon, J. B.; Chusuei, C. C.; Deng, Y. J. Oxidation of chromium(III) to (VI) by manganese oxides. *Soil Sci. Soc. Am. J.* **2002**, *66* (1), 306−315.
(90) Luo, Z. J.; Chatterjee, N. Kinetics of oxidation of Cr(III)-organic complexes by H_2O_2. *Chem. Speciation Bioavailability* **2010**, *22* (1), 25−34.
(91) Duckworth, O. W.; Sposito, G. Siderophore-promoted dissolution of synthetic and biogenic layer-type Mn oxides. *Chem. Geol.* **2007**, *242* (3−4), 497−508.
(92) Pokrovsky, O. S.; Schott, J. Surface chemistry and dissolution kinetics of divalent metal carbonates. *Environ. Sci. Technol.* **2002**, *36* (3), 426−432.

DOI: 10.1021/acs.est.6b05408
Environ. Sci. Technol. 2017, 51, 3223−3232